Kanayim Teshebaeva | Sigrid Roessner | Helmut Echtler
Mahdi Motagh | Hans-Ulrich Wetzel | Bolot Molodbekov

ALOS/PALSAR InSAR Time-Series Analysis for Detecting Very Slow-Moving Landslides in Southern Kyrgyzstan

Suggested citation referring to the original publication:
Remote sensing 7(7) (2015), pp. 8973–8994
DOI http://dx.doi.org/10.3390/rs70708973
ISSN 2072-4292

Remote Sens. **2015**, *7*, 8973-8994; doi:10.3390/rs70708973

OPEN ACCESS

remote sensing

ISSN 2072-4292

www.mdpi.com/journal/remotesensing

Article

ALOS/PALSAR InSAR Time-Series Analysis for Detecting Very Slow-Moving Landslides in Southern Kyrgyzstan

Kanayim Teshebaeva [1,2,*], Sigrid Roessner [1], Helmut Echtler [1,2], Mahdi Motagh [1], Hans-Ulrich Wetzel [1] and Bolot Molodbekov [3]

[1] GFZ German Research Centre for Geosciences, Telegrafenberg, 14473 Potsdam, Germany; E-Mails: sigrid.roessner@gfz-potsdam.de (S.R.); helle@gfz-potsdam.de (H.E.); mahdi.motagh@gfz-potsdam.de (M.M.); hans-ulrich.wetzel@gfz-potsdam.de (H.-U.W.)

[2] Institute of Earth and Environmental Sciences, Universität Potsdam, 14476 Potsdam, Germany

[3] CAIAG Central Asian Institute for Applied Geosciences, Timur-Frunze str.73/2, Bishkek 720027, Kyrgyzstan; E-Mail: b.moldobekov@caiag.kg

* Author to whom correspondence should be addressed; E-Mail: kanayim@gfz-potsdam.de; Tel.: +49-331-288-28888; Fax: +49-331-288-1192.

Academic Editors: Nicolas Baghdadi and Prasad S. Thenkabail

Received: 11 May 2015 / Accepted: 7 July 2015 / Published: 16 July 2015

Abstract: This study focuses on evaluating the potential of ALOS/PALSAR time-series data to analyze the activation of deep-seated landslides in the foothill zone of the high mountain Alai range in the southern Tien Shan (Kyrgyzstan). Most previous field-based landslide investigations have revealed that many landslides have indicators for ongoing slow movements in the form of migrating and newly developing cracks. L-band ALOS/PALSAR data for the period between 2007 and 2010 are available for the 484 km^2 area in this study. We analyzed these data using the Small Baseline Subset (SBAS) time-series technique to assess the surface deformation related to the activation of landslides. We observed up to ±17 mm/year of LOS velocity deformation rates, which were projected along the local steepest slope and resulted in velocity rates of up to −63 mm/year. The obtained rates indicate very slow movement of the deep-seated landslides during the observation time. We also compared these movements with precipitation and earthquake records. The results suggest that the deformation peaks correlate with rainfall in the 3 preceding months and with an earthquake event. Overall, the results of this study indicated the great potential of L-band InSAR time series analysis for

efficient spatiotemporal identification and monitoring of slope activations in this region of high landslide activity in Southern Kyrgyzstan.

Keywords: interferometric SAR (InSAR); small baseline subset (SBAS); time-series; ALOS/PALSAR; deep seated landslide; very slow moving landslide

1. Introduction

Landslides are a widespread phenomenon in mountainous regions affected by ongoing tectonic activity. Additionally, deep-seated landslides represent an especially high risk to the local population because they generally occur in the relatively densely populated foothill zones of the high mountain ranges. They are characterized by a highly variable activity style that comprises both regular and rather continuous slow movements as well as accelerations, which eventually cause sudden slope failures [1]. The velocities of very slow moving landslide are less than 1.6 m/year, according to the velocity classification of Cruden and Varnes, 1996 [2]. In case of deep-seated landslides, the mobilization and downward movement often affects large masses and, thus, represents a potential threat with a high likelihood for catastrophic consequences for nearby populations and infrastructure. Therefore, the continuous monitoring of the state of activity is very important for slopes prone to the formation and reactivation of deep-seated landslides. One way to monitor this is to establish ground-based monitoring systems, which provide detailed information on above-ground and subsurface process characteristics contributing to the principle understanding of the nature of the phenomenon. However, these methods are mostly point-based and are rather limited in the spatial extent of the monitored area, which is especially insufficient if large areas are affected.

On the contrary, the Satellite Synthetic Aperture Radar (SAR) Interferometry (InSAR) technique has evolved as a powerful tool to assess the slope deformation related to the activation of deep-seated landslides [3–6]. With the increasing availability of suitable radar data, advanced time-series analysis techniques have been developed, which allow for the quantitative derivation of spatially variable deformation rates with increasing improvements in the temporal resolution. The resulting satellite InSAR techniques have been successfully applied for the quantitative analysis of landslide activities in a variety of environments [7–12]. A comprehensive review of the current state-of-the-art satellite InSAR-based landslide investigations can be found in Wasowski & Bovenga, 2014 [13].

In our study, the potential of satellite InSAR time-series analysis for quantitative monitoring of slope deformations related to landslide activity is assessed for a study area in Southern Kyrgyzstan, which is part of the tectonically active Tien Shan. This region is situated at the eastern margin of the Fergana Basin, one of the most landslide-prone regions in Central Asia (Figure 1). Deep-seated landslides represent one of the major natural hazards in this densely populated region. Therefore, landslides have been investigated since the 1950s with the aim of improving the understanding of the mechanisms as a main prerequisite for the effective protection of the population [14].

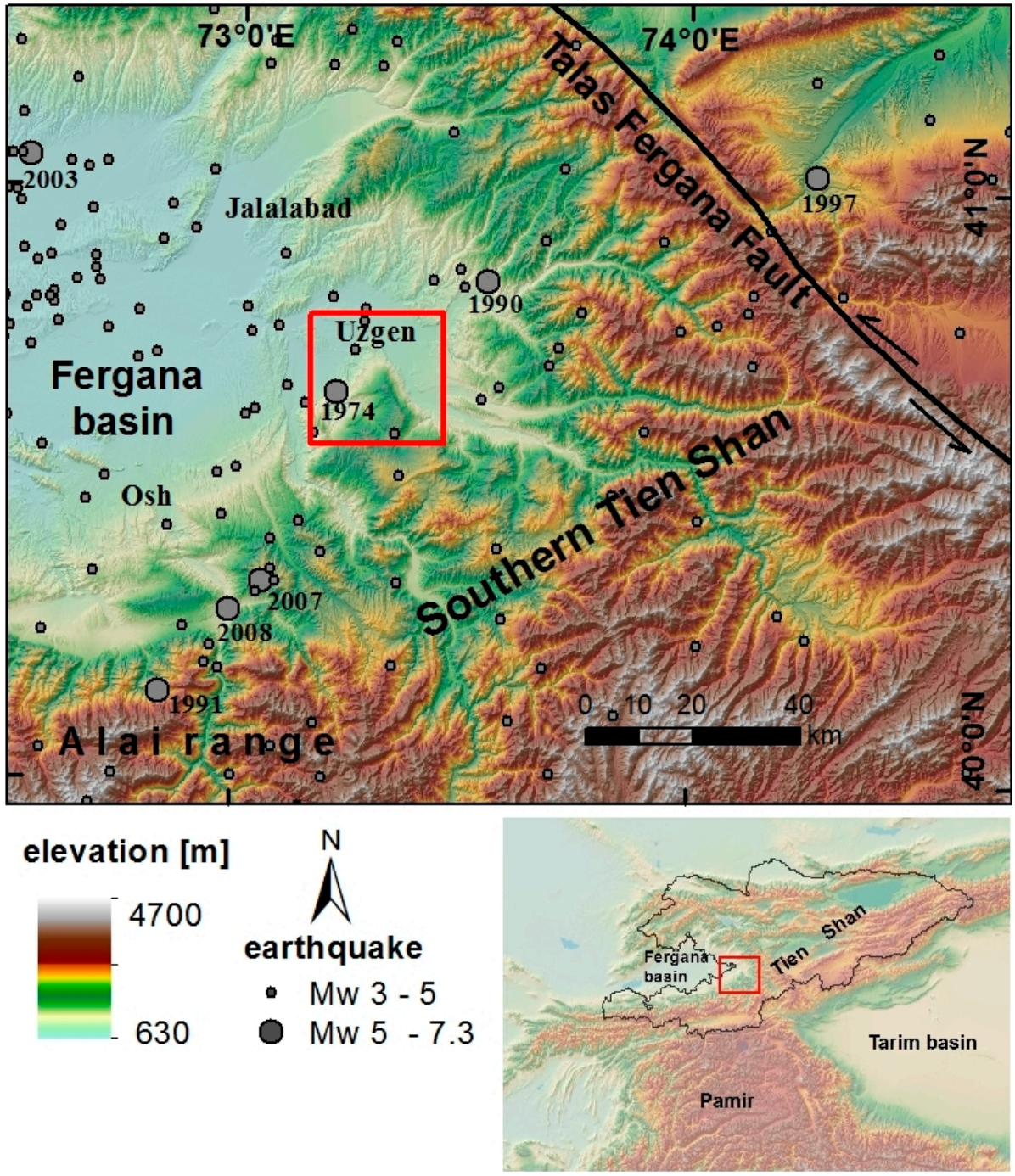

Figure 1. Geographic location of the Uzgen study area in the Southern Tien Shan. The map shows the main structures overlaid on the topography represented by the ASTER GDEM and the red box indicates the study area. The gray circles correspond to the earthquake events contained in the National Earthquake Information Center (NEIC) catalog for the period between 1973 and 2014.

Such investigations have been carried out primarily based on field investigations and have been aided by geological and topographical maps, as well as aerial photographs [14,15]. The use of optical satellite remote-sensing data has allowed for the spatial characterization of the predisposing factors [16,17] and the establishment of a spatially consistent multi-temporal landslide inventory system at a regional scale by integrating landslide information from various sources [18,19].

These investigations have also revealed that most of the landslide prone slopes have been repeatedly affected by mass movements, which has resulted in various stages of the reactivation and enlargement of existing landslide bodies and an extensive relocation of already displaced slope material. Under these conditions, it is very important to obtain the spatiotemporal information concerning the level of activity of the different slope environments that are characterized by high susceptibility to landslide phenomena. Despite the above-described efforts, in the past, this region has lacked rigorous spatial analyses of the landslide activity in relation to the predisposing and triggering factors. Due to the large area affected by landslides and the limited financial means for regular ground-based investigations, satellite InSAR-based techniques and the use of spaceborne monitoring systems may, in general, be powerful tools for detecting areas of increased slope activation. This information is important for spatially- and temporally-differentiated hazard and risk assessments in this region.

To date, few satellite InSAR studies have been performed in Central Asia because of the limited availability of suitable radar data. However, this is changing, following the launch of the ALOS-PALSAR in 2006 and the TerraSAR-X satellites in 2007. In Southern Kyrgyzstan, L-Band ALOS-PALSAR data were used to analyze the 2008 6.5 Mw Nura earthquake [20], whereas X-band TerraSAR descending data represented the basis for detecting the landslide-related surface deformations in the area south of Uzgen [21]. The landslide-related results show that it is possible to derive quantitative deformation rates in areas that were previously affected by landslides, which indicate the reactivation of existing landslides. However, the detection of these reactivations by using short wavelength X-band data has been limited due to the lack of coherence during the winter months and the relatively short data acquisition period [21]. This X-band sensitivity has already been described in other studies, such as Notti *et al.*, 2010 [22].

In this study, we aim to investigate the potential of the longer wavelength L-band ALOS/PALSAR data for the longer-term monitoring of landslide activity in the southern Tien Shan. Methodologically, we focus on a time-series analysis and use the small baseline subset (SBAS) technique as a satellite InSAR approach; this allows for the quantification of the deformation rates of slow-moving landslides and, thus, for the temporal analyses of their stages of activity [23]. In a second step, we analyze the obtained spatial distribution of the deformation velocity rates in relation to the geomorphic setting and the temporal evolution of the observed deformations in relation to the precipitation, temperature and earthquake activity.

2. Study Area

2.1. Geological and Geomorphological Settings

The study area is situated in the transition zone between the Fergana basin and the high-relief Alai range as part of the southern Tien Shan near the town of Uzgen (Figure 1). This region is tectonically active as part of the Indian and Eurasian collision zone [24–26]. Paleozoic and older rocks form the Southern Tien Shan range, and Mesozoic and Cenozoic sediments fill the Fergana basin [27,28]. The geological scheme of Figure 2 shows folded and faulted sedimentary formations that range from the pre-Mesozoic basement to recent fluvial deposits with molasses-type character. These sediments have been folded and faulted as a result of Cenozoic tectonics [27,28].

The Uzgen segment of the mountain front integrates an area of 484 km^2, with elevations ranging from 870 to 2250 m.a.s.l. The area is located within the Kara-Darya river basin and is divided into several hydrographic sub-basins (Figures 1 and 2). The main drainage divides follow the highest elevations forming the boundaries of a triangle-shaped plateau, which is tilted to the WNW; this determines the main drainage direction for most of the study area. As a result, the eastern slope is much higher, with a maximum elevation of 2250 m.a.s.l., than the western slope, which has a maximum elevation of 1800 m.a.s.l. Both slopes are part of the Uzgen mountain front, and the western and eastern detachment areas are characterized by average slopes of 15–20 degrees. Within the west- and east-facing slopes, complex deep-seated slope failures have developed over a long period of time with unknown onsets. They are characterized by deep sliding surfaces, which lead to large initial mass movements. Subsequent reactivations of the displaced masses are characterized by low deformation rates (Figure 2). In the past, their occurrence has been mapped for the selected landslide prone areas by the Ministry of Emergency Situations and by field investigations conducted in cooperation with the GFZ Postdam. Therefore, the study area represents a suitable site for investigating the potential of multi-temporal satellite InSAR techniques to analyze ongoing landslide activity.

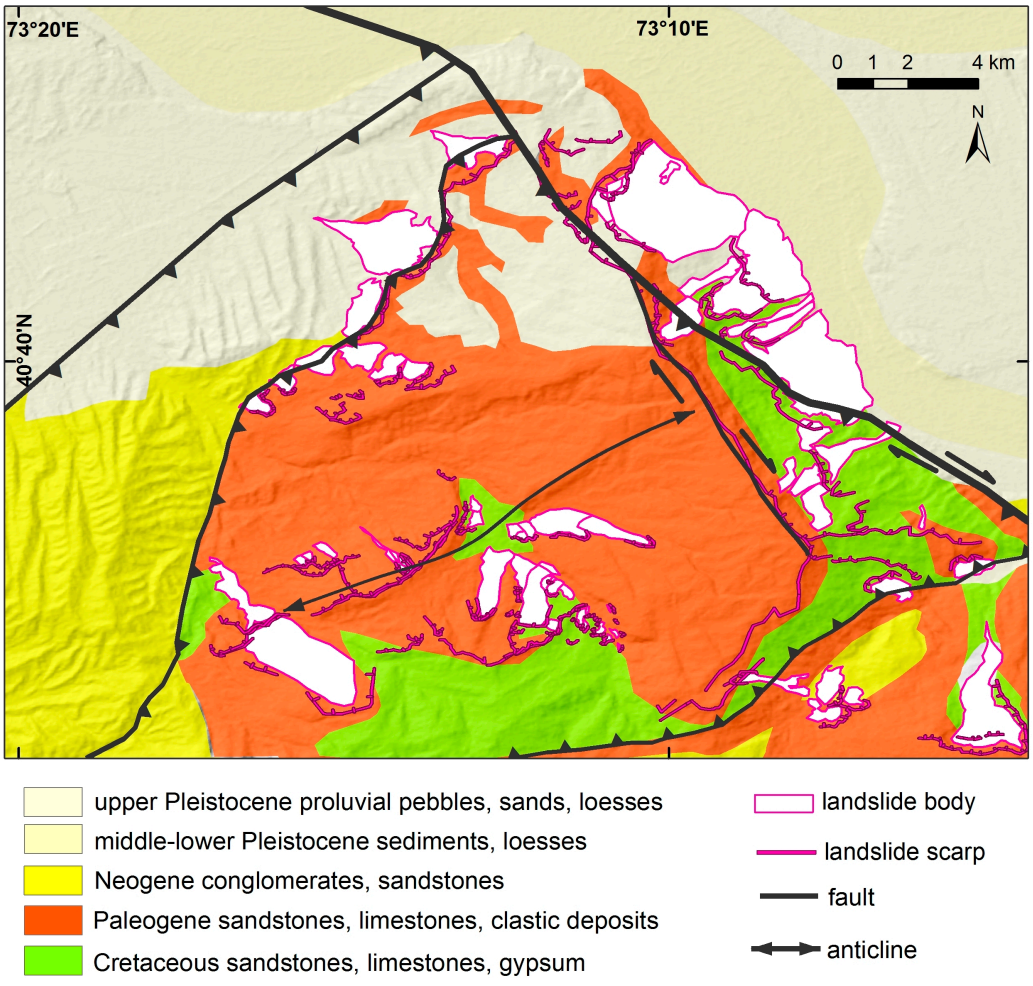

Figure 2. Geological and tectonic map of the study area near Uzgen derived from the 1:200,000 Geological map (1985) and field observations. The A and B profiles cross areas covered by mapped landslides scarps and bodies. The landslides were mapped based on optical satellite remote sensing data and field observations.

2.2. Local Climate and Seismicity

The climate of the region is semi-arid with an average annual precipitation of 350–600 mm/year [14]. The annual precipitation regime has two maxima: one in spring (April and May) and a less pronounced one in fall (October and November) [29]. In winter, the study area has regular snow cover that ranges from 20 to 100 cm in thickness, depending on the elevation and exposition. The average temperature is approximately −10 °C during the winter and +24 °C during the summer [14]. The area is densely populated, with most of the settlements situated in the river valleys. Nearly the entire area is under agricultural use in the form of pastures and agricultural fields. Thus, the vegetation cover consists primarily of grasslands and various agricultural crops, with minor occurrences of trees and bushes.

The region around the Fergana basin is characterized by moderate seismicity [30,31]. According to the NEIC (National Earthquake Information Center, United States Geological Survey) catalogue, approximately 150 earthquakes have been recorded for the period between 1973 and 2014, and the magnitudes of the detected earthquakes are less than 5.2 Mw at the depth ranging from 10 to 40 km. Within the study area, an instrumentally recorded earthquake, the 1974 Kurshab earthquake with a magnitude of 5.1 Mw (Figure 1), occurred near the town of Uzgen during the time period covered by the NEIC catalog.

2.3. The Landslides

Southern Kyrgyzstan is characterized by the frequent occurrence of landslides. Between 1969 and 2010, approximately 4500 landslides were observed in this region [15]. The landslides occurred at elevations ranging from 700 to 2000 m.a.s.l., which are mostly covered by weakly consolidated sediments in the foothill zones of the high mountain ranges of the southern Tien Shan. In this region, progressive mountain building has created a pronounced topographic relief; in combination with a distinct tectonic setting, this forms the spatial framework for the landslide incidents, where the majority of the landslides develop in the form of deep-seated rotational and translational slides [16]. The main period of landslide manifestations is observed in spring, peaking in the months of March and April. The landslide intensity exhibits high interannual variability that is mainly caused by changes in the groundwater levels, which depend on the precipitation characteristics of the preceding winter season. The landslides vary in their size and movement rates [16]. The study area itself is mainly affected by deep-seated landslides, which are characterized by slower movement rates and long periods of activation. These landslides (Figure 2) are prominently situated in Paleogene and Neogene sediments and in Quaternary loess deposits (refs. Map 1:200,000). The thickness of the loess cover does not exceed 30–40 m [32].

In this region, the frequent, but sporadic, occurrence of large landslides results in the temporary formation of dams and the diversion of river courses. It also leads to the extensive damage of settlements and infrastructure and to the loss of human lives. For example, since 1993, more than 250 people have died due to catastrophic slope failures [33]. Satellite remote sensing and field-based investigations of the predisposing factors have revealed that the geological and structural settings play a significant role in the spatial distribution of the landslide occurrence [16,17]. However, there is still limited understanding of the spatiotemporal characteristics of the landslide mechanisms in relation to

the main triggering factors comprising the precipitation and seismicity. In this context, satellite InSAR analysis allows for the quantitative assessment of the slope deformations related to the movement styles and rates.

3. Data and Methodology

3.1. Data

The SAR imagery analyzed in this study consists of 21 ascending L-band ALOS/PALSAR data sets collected between February 2007 and October 2010. The L-band is the transmitting and receiving microwave frequency of the PALSAR, which operates at a wavelength of 23.6 cm with a temporal resolution of 46 days, and the incidence angle of the acquisitions is approximately 38 degrees. The L-band data are capable of partially reaching the ground surface by penetrating through vegetation cover, thus making PALSAR especially suitable for mapping the surface deformations over longer periods of time. The results derived from the ascending L-band data are compared with results that have been obtained from the descending X-band data for the spring-summer period of 2009 (Motagh *et al.*, 2013 [21]). The TerraSAR-X system operates in the X-band (at a wavelength of 3.1 cm) with a temporal resolution of 11 days and an incidence angle of approximately 23 degrees.

We also used ancillary data comprising geological information derived from the 1:200,000 geological map produced by Leningrad State University in 1985; monthly precipitation/temperature data of the Uzgen station for the years 2007 to 2010 recorded by the Kyrgyz Hydrometerological Agency; and seismicity data obtained from the NEIC catalog (1973–2014).

3.2. StaMPS Method

Slow-moving landslides can be detected and analyzed by integrating spaceborne SAR interferometry data with thematic maps and field observations [13]. We used the StaMPS software to obtain the ground deformation [34] by applying the SBAS technique to the interferograms proposed by Berardino *et al.*, 2002 [35]. The SBAS technique uses interferograms with small spatiotemporal baselines to mitigate the de-correlation phenomena of the SAR data and to reduce the Doppler centroid frequency differences [35]. The outcomes of the SBAS analyses are the mean displacement velocity maps and the time series of the displacements of each coherent pixel that can be analyzed for its temporal evolution. The time-series analysis for the study area was performed using the following workflow: (1) the generation of a subset of small baseline interferograms; (2) the selection of slowly de-correlating filtered phase (SDFP) pixels, defined as pixels whose filtered interferometric phase after azimuth and range filtering shows slow de-correlation over short time intervals; (3) the performance of 3-D phase unwrapping of the SDFP pixels; (4) the generation of the time-series and mean velocity deformations according to the coherent pixels; (5) the visualization of the obtained deformation StaMPS results and the export to the GIS environment; (6) the projection of the LOS deformation along the local steepest slope deformation that is a downslope movement, which is then further analyzed with thematic maps. More details on the StaMPS method can be found in the literature [34,36].

3.3. StaMPS Processing

We generated a subset of small baseline interferograms with spatial and temporal baselines smaller than 2560 m and shorter than 950 days, respectively, to maintain better coherence. The key requirement in selecting spatial and temporal baselines is to consider nearly all of the available SAR acquisitions. We analyzed a total of 118 interferograms, of which pixels with a mean coherence greater than 0.35 were selected for the time-series analysis of the study area that was largely covered by a rugged vegetated topography. We removed the topographic effects from the interferograms using the SRTM (Shuttle Radar Topography Mission) DEM, which was available at a spatial resolution of 90 m [37].

We calculated the interferograms in the slant range multi-looking direction to obtain a resolution equal to the sensor-defined spatial resolution. We applied the Goldstein filter to amplify the phase signal of the generated interferograms [38]. Then, we applied three-dimensional unwrapping (Delaunay 3D) to utilize the temporal information [36]. The spatially correlated residuals for each small baseline interferogram were visually inspected to identify the unwrapping problems. Following the identification of the incorrectly unwrapped interferograms, we removed them from the unwrapping process.

We applied least-squares inversion after phase-unwrapping to retrieve the phase with respect to the original master image. We determined the quality and accuracy of the processed data by calculating the DEM error, master atmosphere, and orbit error from both the small baseline and the single master interferograms. The processing of the PALSAR data resulted in a spatial resolution of 15 m. To avoid the use of a subsequent spatial interpolator for generating the final results, we geocoded the data stack of results using a spatial resolution of 25 m. Finally, we obtained the mean velocity displacements for the time period between 2007 and 2010.

3.4. StaMPS Results Visualization and Deformation along the Local Steepest Slope

We visualized the processed StaMPS results using the viStaMPS software [39]. We displayed the LOS velocities by applying a coherence threshold of 0.35 as a threshold for the rugged topography and vegetated study area, which resulted in 17,360 coherent targets for the study area shown in Figure 3. We estimated and removed the spatially correlated DEM error, which includes the error contained in the DEM itself and the error caused by the incorrect mapping of the DEM to the radar coordinates. In addition, we removed the atmospheric phase error for the orbit and master scenes. Then, we defined the 22 km by 22 km final subset of the study area shown in Figure 3 based on the spatial distribution of the coherent targets. Finally, we exported the point velocity displacements of these targets into a GIS environment for the further analysis of the obtained ground deformations.

The SBAS-retrieved deformation values represent the one-dimensional LOS projection of the actual movement of the Earth's surface. To overcome the differences between the ground geometry and the LOS direction, we projected the LOS deformations into the direction of the down slope movements [40]. We converted the LOS velocity deformation rates into downslope velocity deformation rates (Vslope) [41,42]. To transform the LOS direction into the down slope direction, we needed information about the unit LOS vectors and the slopes. For the unit LOS vectors, we used the incidence angle and the flight azimuth of the satellite. In addition, we employed the slope angle and the slope azimuth for the study area (Figure 4), including the calculations of the slope and azimuth

values using the ASTER GDEM2, because the 30-m spatial resolution is better than the 90-m resolution of the SRTM-DEM.

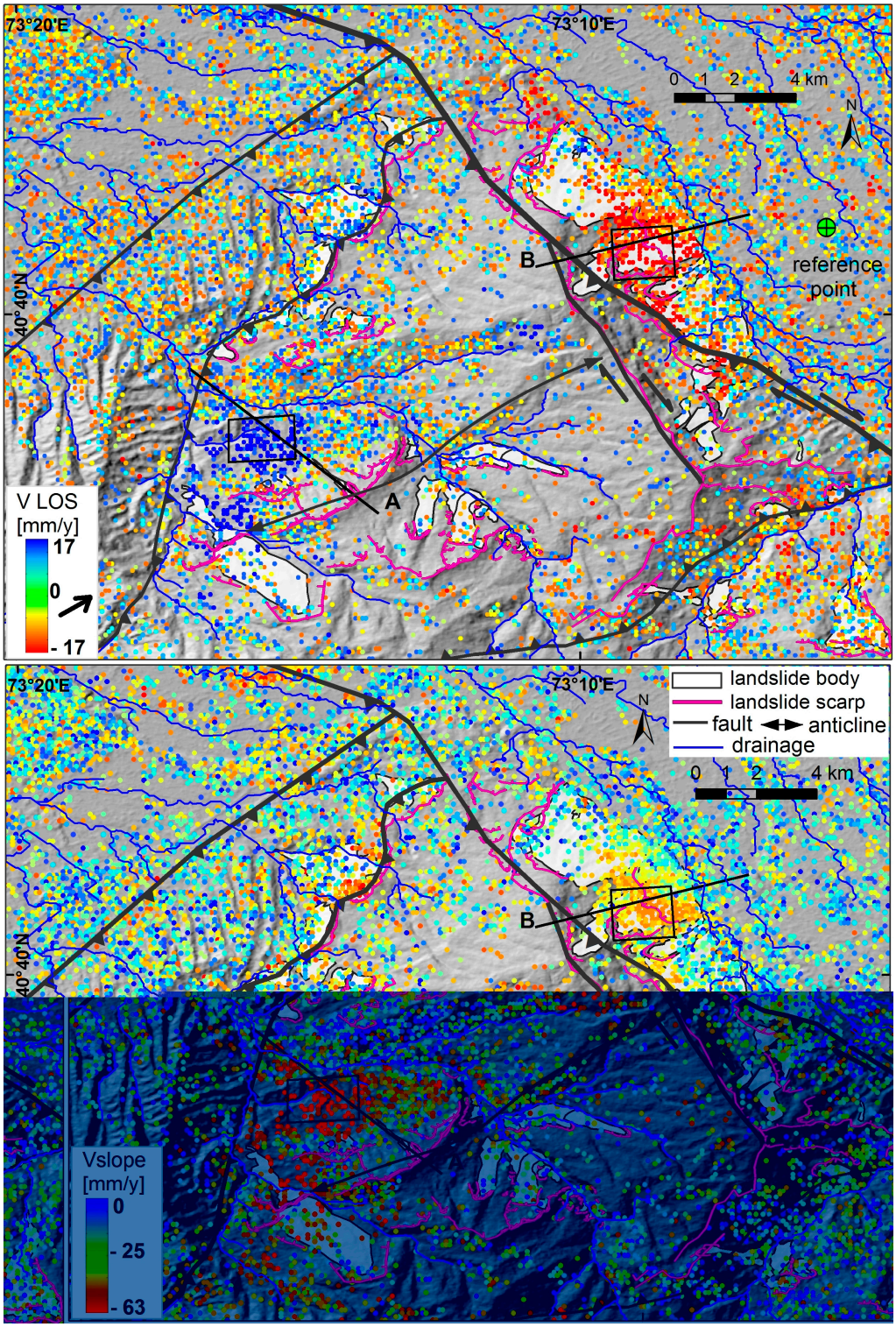

Figure 3. Map of mean velocity deformation rates (mm/year) in LOS direction (**upper panel**) and projected to downslope Vslope velocity deformation rates (mm/year) (**lower panel**) obtained for spatially distinct coherent targets (color dots) for the time period between 2007 and 2010. The black boxes represent the spatial subsets for the detailed temporal analysis of slope deformation patterns.

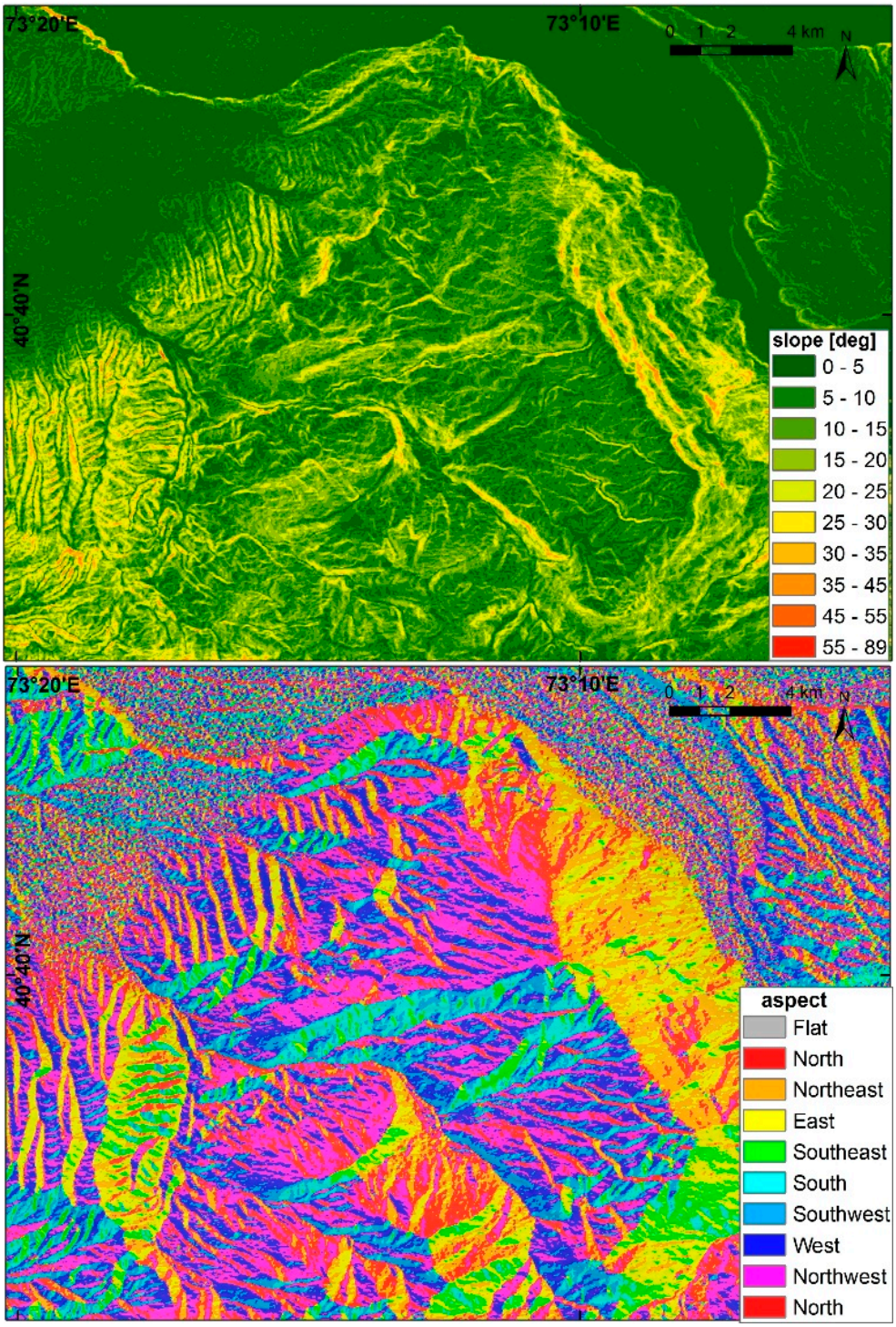

Figure 4. Slope and aspect map of the study area calculated based on ASTER GDEM2.

4. SBAS Results and Interpretation

4.1. Spatial Distribution of Landslide Deformation

The processed 21 ALOS/PALSAR L-band scenes cover a time period of four years (2007–2010). The obtained SBAS results were derived for 17,360 coherent targets situated in the 484-km^2 subset of the Uzgen mountain front (Figure 3). We selected a reference point (Figure 3) that was characterized by high coherence and whose deformation behavior was known *a priori* as a non-deforming zone.

This zone represents the stable foreland outside the tectonically active area, as indicated by a younger geological surface (Figure 2). From the results shown in Figure 3, we identified a selection of benchmarks located in the non-deforming zone, which represent the area around the reference point. For this benchmark, we superimposed the line of sight-projected leveling measurements and the value of the standard deviation, ±4 mm/year. We consider this value to be the standard error that must be used in further interpretations of the results.

The obtained SBAS results only show displacements where the surface moves towards or away from the satellite along the line of sight. The L-band wavelength maintains good coherence over the longer periods of time (up to one year) and thus provides longer-term information of the surface deformations related to the landslide processes. The results of the ascending interferograms are more sensitive to the mass movements that occur on the eastward facing slopes. Our satellite InSAR results show the deformations in areas that were formerly affected by landslides. The velocity rates in the LOS direction are up to ±17 mm/year (the red to blue color range in Figure 3). The most pronounced surface deformation signals detected in this study are located at different slope orientations: one signal is observed on the east slope, and the other is found on the west slope (Figure 3). To homogenize these differences, we project the LOS to the downslope, and we obtain the Vslope landslide movements.

The SBAS-observed downslope velocity deformation rates (Vslope) range from >0 to 63 mm/year (Figure 3). Among the coherent locations characterized by high downslope deformation rates, we identified two major signals. One is situated on the (1) western slope, and the other is on the (2) eastern slope; both were determined using the downslope velocity values (Figure 3).

(1) At the western slope we observed downslope velocity deformation rates of up to −63 mm/year (Figure 3). The observed signal covers an area that is up to 4 km wide and ranges in elevation from 1800 m.a.s.l to 1100 m.a.s.l. over a horizontal distance of approximately 6 km, which results in an average slope of 15 degrees. Increased deformations on the western slope mainly occur in the area represented by profile A (Figure 5), which had not been identified previously as an active landslide area. However, these locations are situated in the downslope vicinity of morphologically distinct scarps, which indicate the presence of relict landslide masses in this area [43] (Figure 5).

(2) On the eastern slope, we observed downslope deformation velocity rates of up to −35 mm/year, which occur primarily in the area of already-existing landslide bodies (Figure 3). In this area, the presence of geomorphologically distinct landslide features allowed for the mapping of individual landslide bodies using optical remote-sensing data and field investigations (Figures 5 and 6).

The eastern slope is characterized by several fresh scarps and surface breaks, which indicate recent downslope movements and were documented during field work in September 2011 (Figure 6). The observed signal is up to 5 km wide and covers an area with elevations ranging from 1900 m.a.b.s.l. and 1000 m.a.b.s.l., with a horizontal distance of approximately 5 km, thus resulting in an average slope of 17 degrees. On the eastern slope, represented by profile B (Figure 6), coherent locations that are characterized by increased deformation spatially coincide with previously mapped landslides, which indicate ongoing landslide activity during the analysis period.

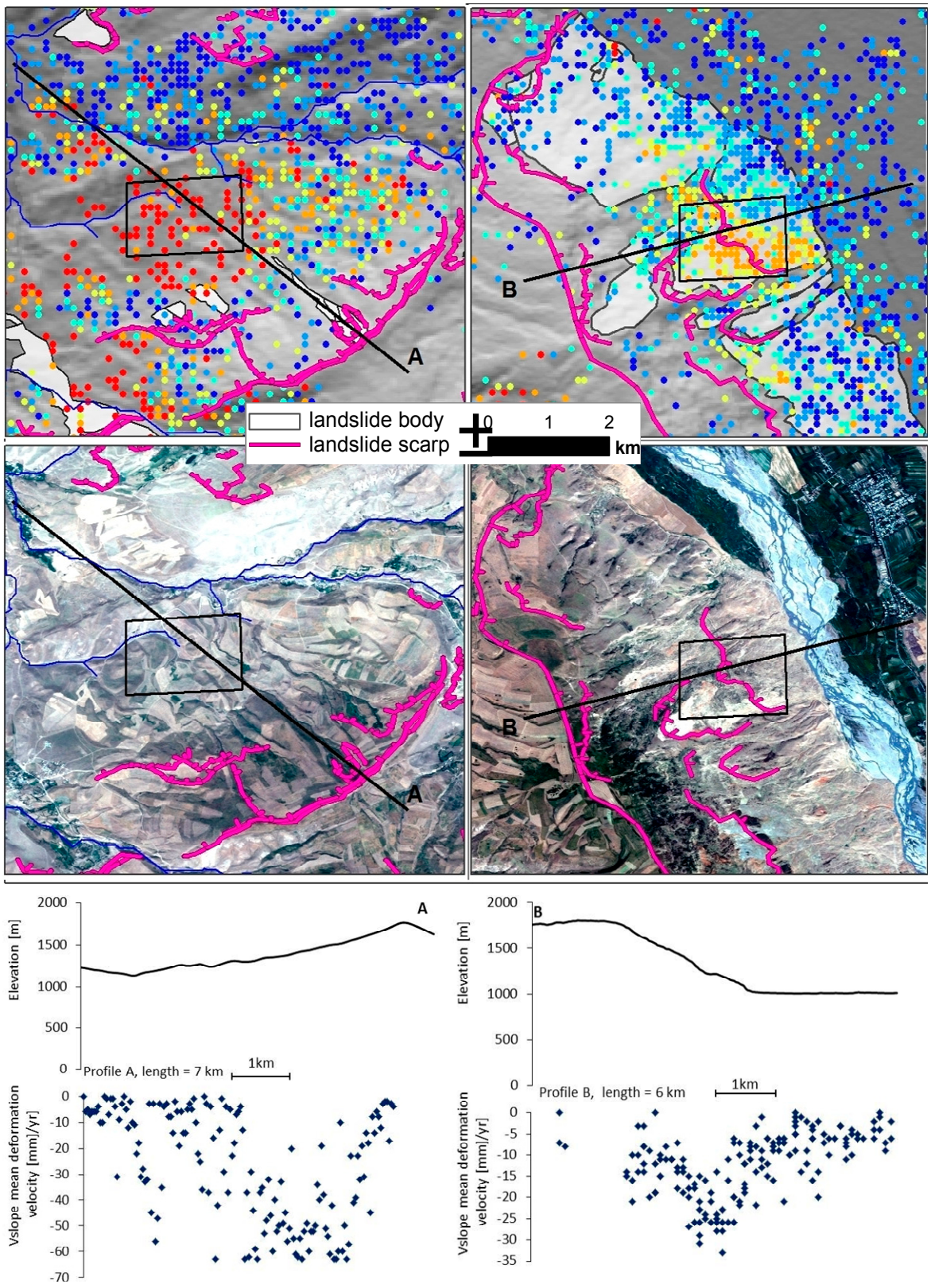

Figure 5. Map of Vslope deformations drawn across the west (profile A) and east (profile B) (upper panel). The middle panel shows the coverage of the area by optical RapidEye data which were acquired in August 2014. The lower panels depict profile information of the down slope deformations and elevation data.

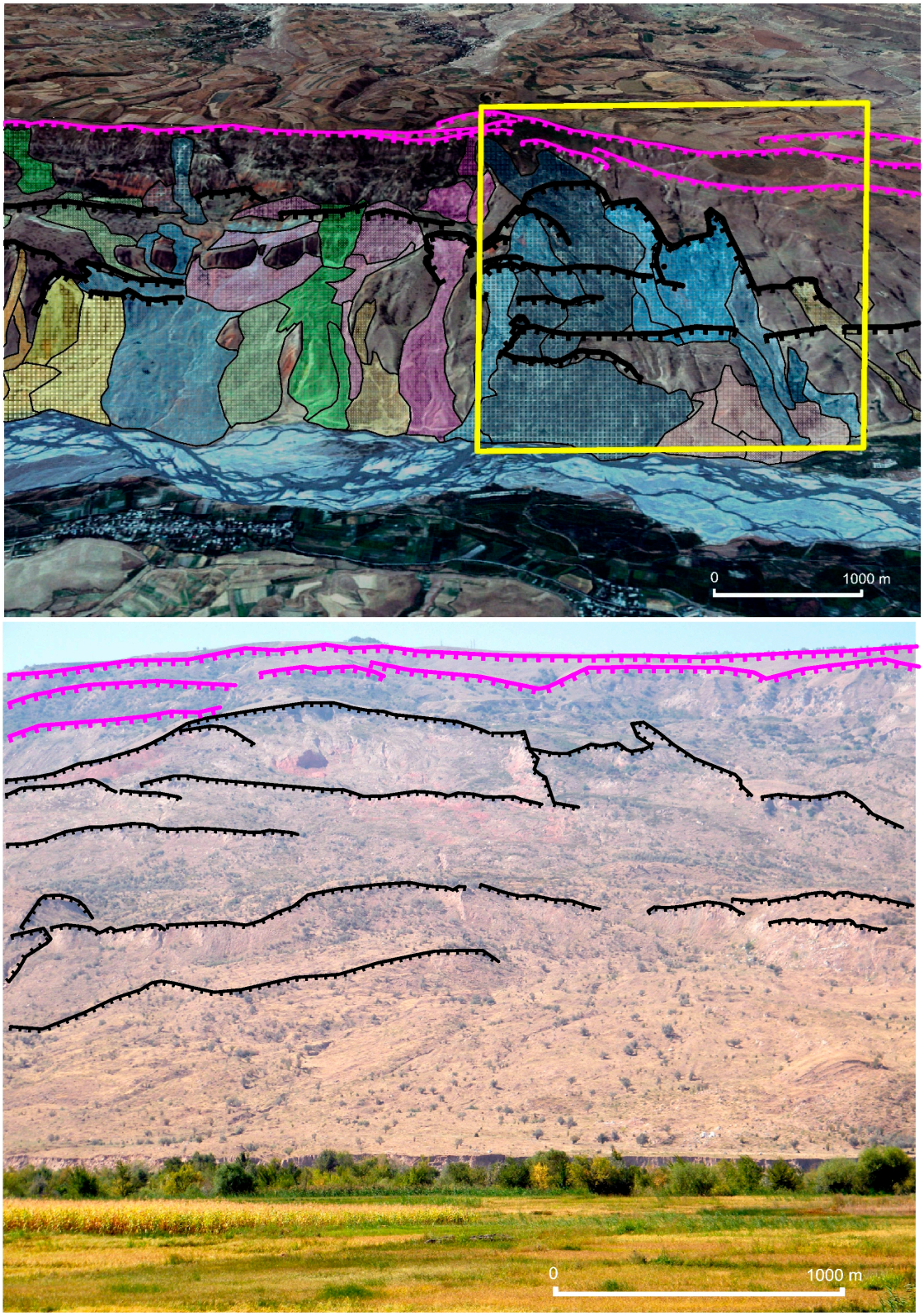

Figure 6. Mapped landslide complexes derived from optical remote sensing data and field observations. Perspective view of the eastern slope (Figure 4) overlaid by Rapid Eye imagery acquired on the 5 April 2011 (**upper panel**) and field photo (yellow box) taken on 11 September 2012 (**lower panel**). The individual landslide bodies are indicated by different colors, the main scarps are depicted in magenta and secondary scarps are depicted in black.

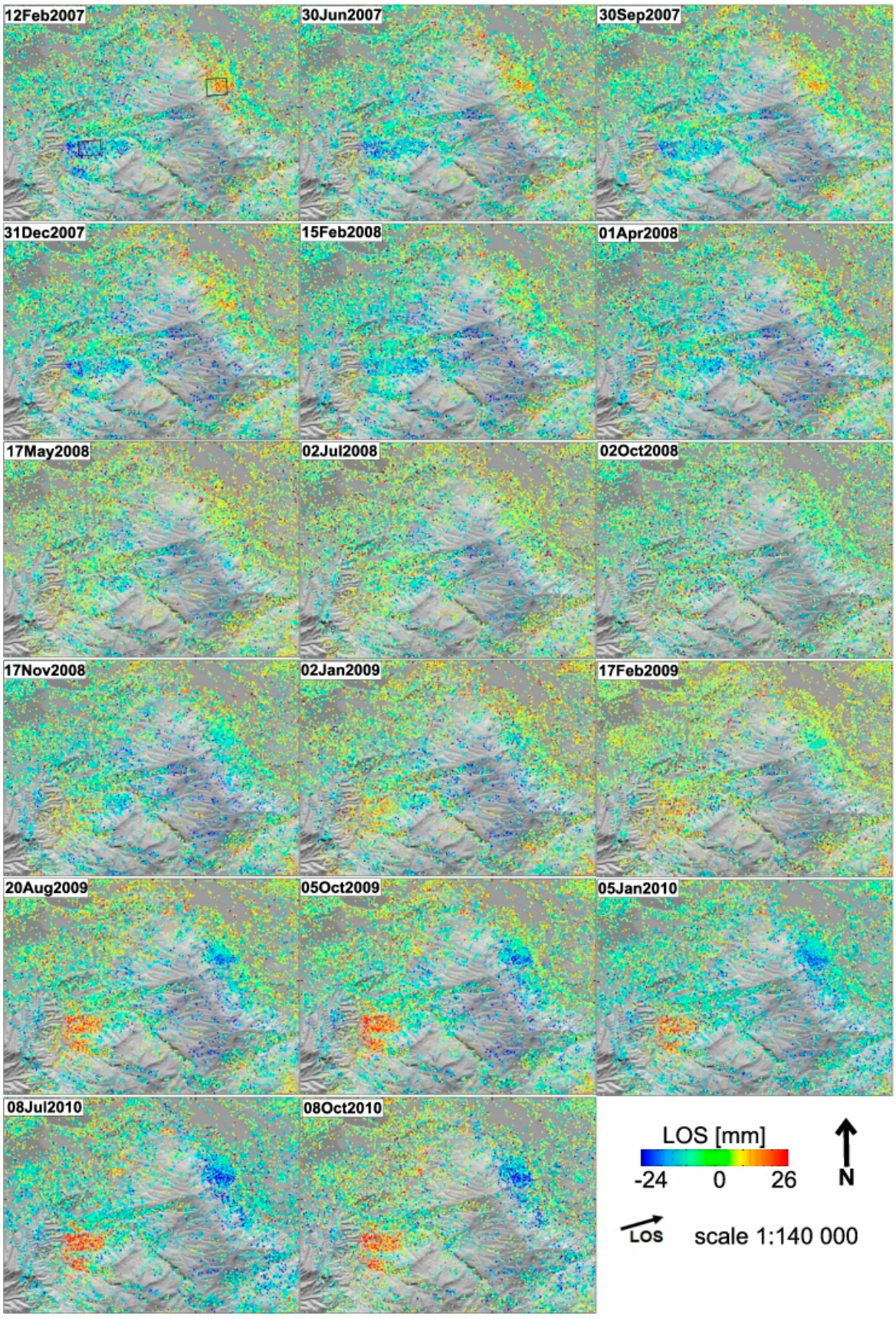

Figure 7. Time-series LOS displacement map for the period between 2007 and 2010, the reference date is 2nd July 2008. The data inside of black boxes presented in time-series profiles in Figure 8.

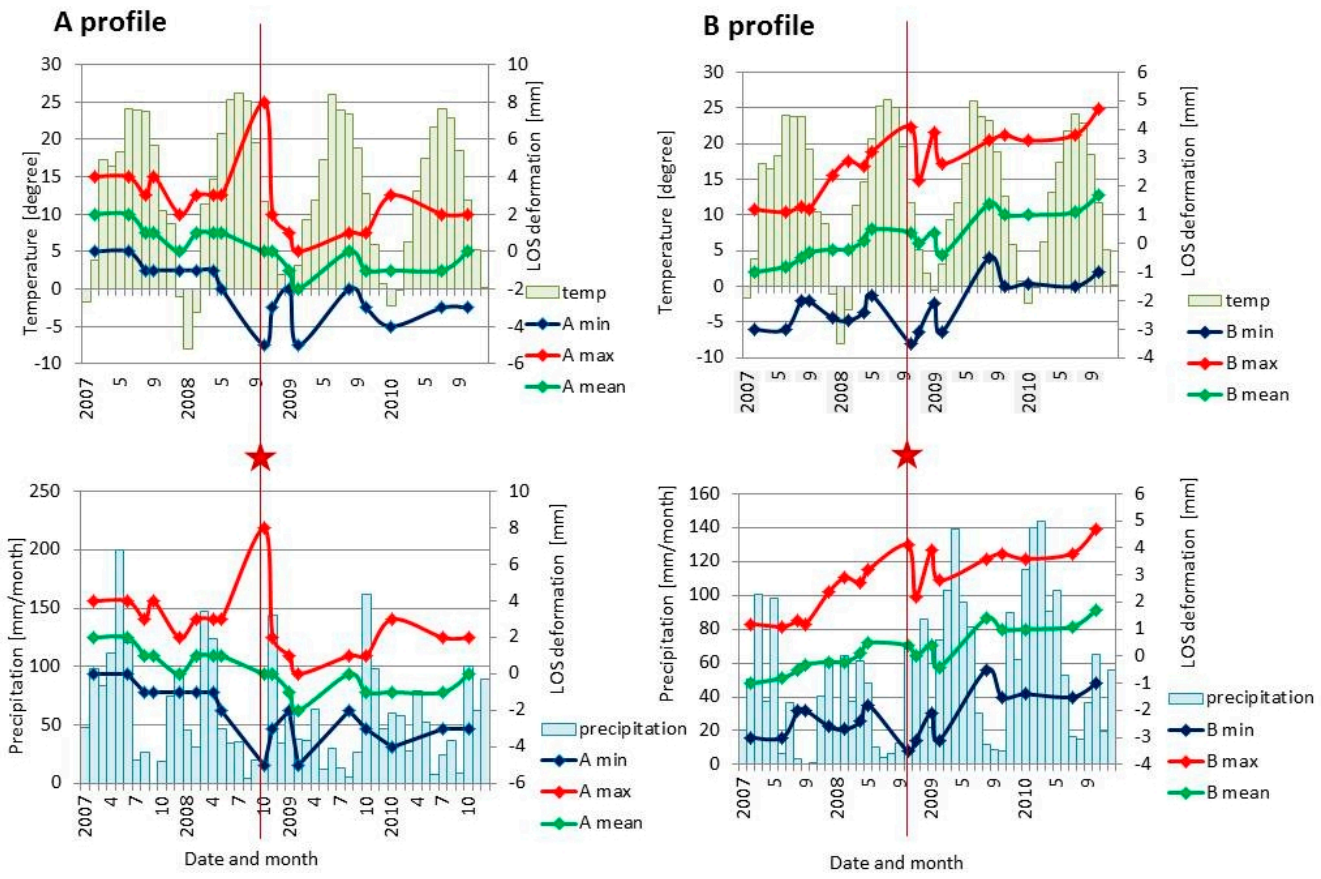

Figure 8. Time-series LOS displacement along profiles A and B for the period between 2007 and 2010 plotted against monthly sums of precipitation and monthly averages of temperature. The peak of the deformation on 2 October 2008 coincides with the Mw 4.1 earthquake of 26 September 2008.

4.2. Temporal Evolution of Landslide Deformation

In addition to analyzing the mean deformation rates (Section 4.1), we investigated the temporal evolution of the detected deformations between 2007 and 2010 based on the time-series of date-to-date LOS displacements (Figure 7). For this purpose, we de-trended our time-series data to exclude any linear trends that could influence the subsequent analysis. To understand the temporal evolution of the detected deformation, we analyzed the data in relation to the temperature, precipitation and seismicity. For this purpose, we constructed 1.6-km-wide swath profiles depicted as black boxes in Figure 3, and we calculated the minimum, maximum, and average deformation values that occurred within these areas to check the signal stability. In Figure 8, we plotted the values of the de-trended date-to-date deformation time series for the period 2007–2010 against the available time-series data for the precipitation (monthly sums) and the temperature (monthly means) as well as the temporal occurrence of the October 2008 Mw 4.1 earthquake. For both profiles, the observed LOS displacements indicate continuous movements in the LOS direction (Figures 7 and 8). Profiles A and B (Figure 6) show differences in the temporal evolution between the deformation signals. Based on the plots, we compared the LOS displacement signals with the temperature and precipitation. The temporal evolution of the deformation along profile A shows a continuous LOS deformation with a distinct peak

in October 2008 (Figure 8). The profile B plots also indicate a three-month correlation between the precipitation and the increased deformation rates. Comparing the time series of deformation with the time series of temperature data for profiles A and B (Figure 8) shows that our observed time-series LOS deformation signal does not correlate with the changes in temperature. This observation suggests that the slope instabilities in this area are not related to freezing and thawing processes.

5. Discussion

5.1. SBAS Results Assessment

In general, the quality of multi-temporal interferometry is checked using cross-comparisons and ground truth [13]. We apply the approach of comparing the ascending L-band PALSAR observations with the descending X-band TSX observations, which have been derived for the same study area [21]. Our L-band PALSAR results represent the cumulative surface displacements for the analyzed time period 2007–2010, which indicate reactivations in the larger parts of the east and west slopes of the Uzgen area. The analysis of the same Uzgen area using descending X-band TSX data showed episodic cm-scale displacement features in the area of the west slope only during the spring-summer period of 2009. Motagh *et al.*, 2013 [21] excluded the winter season from their analysis due to a lack of coherence caused by the strong de-correlation of the InSAR signal. The interferometric coherence degraded quickly in the winter and early spring period, presumably due to continuous snow cover, rainfall or the start of vegetation growth. The results from the ascending L-band data spatially correlate with the results obtained from the descending X-band data. Our L-band results and X-band results are complementary; thus, the L-band data are more suitable for long-term monitoring and the X-band data for short-term monitoring of unstable slopes in the mountainous regions of Southern Kyrgyzstan. Similar observations of the performance of L-band ALOS data compared with X-band and C-band data have been made in the Tena Valley of the Central Spanish Pyrenees [3]. However, the X-band data preserve the spatial details and short-term slope deformations well**.** Therefore, they exhibit good potential for the rapid assessment of changes that might occur before or after large slope failures, including the detection of damages related to these failures through more detailed analyses of areas characterized by the loss of or decrease in coherence [13,22].

5.2. Downslope Deformations of Landslides

The downslope velocity deformation rates of up to -63 mm/year (Section 4.1) lie in the category of very slow moving landslides [1,2]. Our analyses show that our detected areas of activation within the landslide-prone slopes are located in areas characterized by a slope angle of 15–17 degrees, which is much smaller than the ALOS/PALSAR look angle of 38 degrees. Therefore, landslides can be detected without limitations [9,11,44]. Thus, in the area of the Uzgen mountain front, the landslide-prone slopes exhibit the best geometry for monitoring based on the use of L-Band ALOS/PALSAR data. The eastern slope reveals a predominant movement in the NE direction, which is perpendicular to the orientation of the neighboring river valley. The western slope is characterized by a predominant NNW movement direction, which is parallel to the orientation of the neighboring river valley. Compared with the eastern slope, the obtained velocity rates are approximately 45% higher for the

western slope (Figure 3). The western slopes surface deformation occurs in an area underlain by Paleogene clastics. Despite the absence of unequivocal geomorphological indicators of ongoing landslide activity, the high deformation rates on the western slope suggest the reactivation of an ancient landslide body. Compared with the western slope, the eastern slope has been well documented and mapped because of its high ongoing landslide activity. The origins of these slope failures are deep-seated landslides, where the sliding plane has formed along the boundary between the Cretaceous rocks and the unconformable, overlying Pleistocene sediments. The local authorities have confirmed protracted landslides in this area (oral communication, Ministry of Emergency Situations). The most recent major failures in this area occurred in 1988 and in the period between 2003 and 2005, and they coincide with phases of high landslide activity in Southern Kyrgyzstan. The temporal evolution of the landslide activity in this area derived from the optical satellite remote-sensing time-series data exhibit regularly reoccurring landslide activity between 1990 and 2013 [19]. The SBAS results suggest that the already displaced landslide masses have been subject to subsequent reactivations, which also affect the youngest Pleistocene deposits. Comparable findings of the ALOS/PALSAR-derived downslope velocities of the very slow moving landslides have been observed in Spain [11] and in Three Gorges in China [8].

5.3. Potential Controls on Landslide Activity

The analyzed deformation time-series reveal the presence of temporal changes of up to a few mm/year in the velocity of the landslide movements for the west and east slopes. The analysis presented in Section 4.2 shows that the observed signals do correlate with an earthquake and precipitation but do not correlate with temperature. In general, the low velocity rates of the surface deformations on the slopes may arise from a wide variety of causes and are thus not simple to interpret [13,45]. However, in case of landslides, the most significant impacts are often those related to (1) climatic variations and their influence on hydrogeology [13] or to the deep-seated landslides of the folded and faulted inherited tectonic structures with (2) moderate seismicity in the unconsolidated sediments [46].

(1) The east slope surface deformation patterns reconstructed along profile B show some seasonality (Figure 8). The deformation acceleration is most likely driven by gravitational slope processes, which are influenced by the overall steeper relief and by changes in the ground water level that result from the integrative amount of precipitation occurring within the last three months prior to the observed deformation increase. This result is in accordance with the observations provided by the Ministry of Extreme Emergency [14]. Similar findings of the landslide seasonality have been reported from Northern California for the area of the Berkeley Hills slide [44]. Due to low temporal resolution of the ALOS/PALSAR data, it is impossible to determine a more precise correlation between the landslide activation and precipitation [44].

(2) In the area of the west slope, the observed high deformation rates are most likely related to seismic activity, which primarily manifests itself along the local faults. The available seismicity data for the area show that the distinct deformation peak observed in profile A can be linked to the Mw 4.1 earthquake, which occurred on 26 September 2008, at a 30-km distance from the local thrust system. Moreover, that area had been previously affected by an Mw 5.1 earthquake in February 1974. At that

time, mass movements following the earthquake had also been reported [47]. In the area of the west slope, the LOS time-series deformation shows correlation with the seismic activity, which likely leads to the gravitational reactivation of old landslide structures in the vicinity of a tectonically active fault.

Moreover, our deformation results have revealed different activity stages in an area of ongoing landslide activity (east slope) as well as the activation of an area that has not been affected by visible landslide activity in the recent past (west slope). These findings are in agreement with already existing knowledge of landslide processes in this area [16], thus leading to the observation that the deep-seated landslides occurring in this area are the result of complex interplay between hydrometeorological factors, the local geological setting and seismicity.

6. Conclusions

In this study, we show the potential of satellite InSAR analysis based on L-band ALOS/PALSAR imagery to detect and map very slow-moving landslides. Satellite InSAR time-series analysis has resulted in very slow and temporally-uniform landslide movements, which have occurred during the time period from 2007 to 2010. Further analyses of the temporal evolution of these very slow-moving landslide show that the local seismicity and the prior three-month precipitation amounts contribute to the activation of landslide prone slopes. Most of the obtained deformation represents the reactivation of already existing landslides; whereas the spatial occurrence is controlled by the folded and faulted inherited tectonic structures within the weakly consolidated sediments. The obtained L-band results correlate spatially with the X-band results obtained in an earlier study [21], which indicates continuous landslide activity in the area of the Uzgen mountain front. Thus, it can be concluded that the results obtained by the two independent studies are consistent and can be used concurrently to assess both short- and longer-term landslide activity in this area. Both studies have shown the great potential of satellite InSAR analysis for the regular monitoring of landslide activity along the widespread landslide prone slopes in this region. The observed deformations represent important information, which can be integrated using dynamic approaches for hazard assessment. Thus, our results show that L-band missions are of great importance for the longer-term monitoring of landslide activity in mountainous regions. In this context, new opportunities have been created from the recently launched PALSAR-2 and Sentinel-1 missions. In the future, the radar remote-sensing data acquisition capabilities will greatly improve for areas such as Central Asia; this will increase the opportunity for the development of operational satellite InSAR-based monitoring systems, which are complementary to ground-based slope observations. The combined analyses of the obtained SBAS results with additional landslide-related information will support regular process monitoring as part of a quantitative hazard and risk assessment as well as an early warning system in Southern Kyrgyzstan and other landslide prone regions of Central Asia.

Acknowledgments

We thank Manfred Strecker, Bodo Bookhagen and Oliver Korup for valuable discussions, which helped to improve the content of the paper. This research was funded by the Volkswagen foundation within the frame of the LUCA (Land Use, Ecosystem Services and Human Welfare in Central Asia) post-graduate program. The work was also supported by the German Research Foundation (DFG)

under the auspices of the Graduate School GRK1364 “Shaping Earth’s Surface in a variable Environment” (Strecker STR 373/18-1) and the Central Asia and Afghanistan Research Fellowship (CAARF). The ALOS data for this study were provided by the Japanese Aerospace Agency (JAXA) through the research proposal P610.

Author Contributions

Kanayim Teshebaeva performed the analyses and interpretation, she wrote the paper with contributions from Sigrid Roessner, Helmut Echtler and Mahdi Motagh. Helmut Echtler contributed the geologic and the tectonic aspects of the paper. Mahdi Motagh helped with the InSAR methodology. Hans-Ulrich Wetzel and Bolot Moldobekov contributed landslide information and mapping as well as field observations.

Conflicts of Interest

The authors declare no conflict of interest.

References

1. Hungr, O.; Leroueil, S.; Picarelli, L. The varnes classification of landslide types, an update. *Landslides* **2014**, *11*, 167–194.
2. Cruden, D.; Varnes, D. Landslide types and processes. In *Landslides: Investigation and Mitigation*; Turner, A.K., Schuster, R.L., Eds.; National Academy Press: Washington, DC, USA, 1996; pp. 36–75.
3. Herrera, G.; Gutierrez, F.; Garcia-Davalillo, J.C.; Guerrero, J.; Notti, D.; Galve, J.P.; Fernandez-Merodo, J.A.; Cooksley, G. Multi-sensor advanced DInSAR monitoring of very slow landslides: The tena valley case study (central Spanish Pyrenees). *Remote Sens. Environ.* **2013**, *128*, 31–43.
4. Tolomei, C.; Taramelli, A.; Moro, M.; Saroli, M.; Aringoli, D.; Salvi, S. Analysis of the deep-seated gravitational slope deformations over Mt. Frascare (central Italy) with geomorphological assessment and DInSAR approaches. *Geomorphology* **2013**, *201*, 281–292.
5. Calo, F.; Ardizzone, F.; Castaldo, R.; Lollino, P.; Tizzani, P.; Guzzetti, F.; Lanari, R.; Angeli, M.G.; Pontoni, F.; Manunta, M. Enhanced landslide investigations through advanced DInSAR techniques: The ivancich case study, Assisi, Italy. *Remote Sens. Environ.* **2014**, *142*, 69–82.
6. Castaldo, R.; Tizzani, P.; Lollino, P.; Calò, F.; Ardizzone, F.; Manunta, M.; Guzzetti, F.; Lanari, R. The ivancich active landslide process (Assisi, Central Italy) analysed via numerical modeling jointly optimized by DInSAR and inclinometric data. In *Engineering Geology for Society and Territory*; Lollino, G., Giordan, D., Crosta, G.B., Corominas, J., Azzam, R., Wasowski, J., Sciarra, N., Eds.; Springer: Berlin, Germany, 2015; Volume 2, pp. 1513–1517.
7. Tofani, V.; Raspini, F.; Catani, F.; Casagli, N. Persistent Scatterer Interferometry (PSI) technique for landslide characterization and monitoring. *Remote Sens.* **2013**, *5*, 1045–1065.
8. Tantianuparp, P.; Shi, X.; Zhang, L.; Balz, T.; Liao, M. Characterization of landslide deformations in three gorges area using multiple InSAR data stacks. *Remote Sens.* **2013**, *5*, 2704–2719.

9. Sun, Q.; Zhang, L.; Ding, X.; Hu, J.; Liang, H. Investigation of slow-moving landslides from ALOS/PALSAR images with TCPInSAR: A case study of Oso, USA. *Remote Sens.* **2014**, *7*, 72–88.
10. Lu, P.; Bai, S.B.; Casagli, N. Investigating spatial patterns of persistent scatterer interferometry point targets and landslide occurrences in the Arno River Basin. *Remote Sens.* **2014**, *6*, 6817–6843.
11. Bianchini, S.; Herrera, G.; Mateos, R.M.; Notti, D.; Garcia, I.; Mora, O.; Moretti, S. Landslide activity maps generation by means of persistent scatterer interferometry. *Remote Sens.* **2013**, *5*, 6198–6222.
12. Akbarimehr, M.; Motagh, M.; Haghshenas-Haghighi, M. Slope stability assessment of the sarcheshmeh landslide, northeast Iran, investigated using InSAR and GPS observations. *Remote Sens.* **2013**, *5*, 3681–3700.
13. Wasowski, J.; Bovenga, F. Investigating landslides and unstable slopes with satellite multi temporal interferometry: Current issues and future perspectives. *Eng. Geol.* **2014**, *174*, 103–138.
14. Yerokhin, S.A. *Investigation of Landslide Occurence in Osh and Djalalabad Provinces of the Kyrgyz Republic*; Institute of Geology: Bishkek, Kyrgyzstan, 1999.
15. Ibatulin, K.V. *Monitoring of Landslides in Kyrgyzstan*; Ministry of Emergency Situations of the Kyrgyz Republic: Bishkek, Kyrgyzstan, 2011. (in Russian)
16. Roessner, S.; Wetzel, H.; Kaufmann, H.; Sarnagoev, A. Potential of satellite remote sensing and GIS for landslide hazard assessment in southern Kyrgyzstan (Central Asia). *Nat. Hazards* **2005**, *35*, 395–416.
17. Wetzel, H.U.; Roessner, S.; Sarnagoev, A. Remote sensing and GIS based geological mapping for assessment of landslide hazard in southern Kyrgyzstan (Central Asia). In *Management Information Systems 2000: GIS and Remote Sensing*; WIT Press: Southampton, UK, 2000; pp. 355–366.
18. Golovko, D.; Roessner, S.; Behling, R.; Wetzel, H.-U.; Kleinschmit, B. Development of multi-temporal landslide inventory information system for southern Kyrgyzstan using GIS and satellite remote sensing. *Photogramm. Fernerkund. Geoinf.* **2015**, *2015*, 157–172.
19. Behling, R.; Roessner, S.; Kaufmann, H.; Kleinschmit, B. Automated spatiotemporal landslide mapping over large areas using rapideye time series data. *Remote Sens.* **2014**, *6*, 8026–8055.
20. Teshebaeva, K.; Sudhaus, H.; Echtler, H.; Schurr, B.; Roessner, S. Strain partitioning at the eastern Pamir-Alai revealed through SAR data analysis of the 2008 Nura earthquake. *Geophys. J. Int.* **2014**, *198*, 760–774.
21. Motagh, M.; Wetzel, H.U.; Roessner, S.; Kaufmann, H. A Terrasar-X InSAR study of landslides in southern Kyrgyzstan, Central Asia. *Remote Sens. Lett.* **2013**, *4*, 657–666.
22. Notti, D.; Davalillo, J.C.; Herrera, G.; Mora, O. Assessment of the performance of X-band satellite radar data for landslide mapping and monitoring: Upper Tena Valley case study. *Nat. Hazard Earth Syst.* **2010**, *10*, 1865–1875.
23. Lanari, R.; Casu, F.; Manzo, M.; Zeni, G.; Berardino, P.; Manunta, M.; Pepe, A. An overview of the small baseline subset algorithm: A DInSAR technique for surface deformation analysis. *Pure Appl. Geophys.* **2007**, *164*, 637–661.

24. Reigber, C.; Michel, G.W.; Galas, R.; Angermann, D.; Klotz, J.; Chen, J.Y.; Papschev, A.; Arslanov, R.; Tzurkov, V.E.; Ishanov, M.C. New space geodetic constraints on the distribution of deformation in Central Asia. *Earth Planet. Sci. Lett.* **2001**, *191*, 157–165.
25. Strecker, M.; Frisch, W.; Hamburger, M.; Ratschbacher, L.; Semiletkin, S.; Zamoruyev, A.; Sturchio, N. Quaternary deformation in the eastern Pamirs, Tadzhikistan and Kyrgyzstan. *Tectonics* **1995**, *14*, 1061–1079.
26. Zubovich, A.; Wang, X.; Scherba, Y.; Schelochkov, G.; Reilinger, R.; Reigber, C.; Mosienko, O.; Molnar, P.; Michajljow, W.; Makarov, V.; *et al*. GPS velocity field for the Tien Shan and surrounding regions. *Tectonics* **2010**, *29*, doi:10.1029/2010TC002772.
27. Cobbold, P.; Sadybakasov, E.; Thomas, J. Cenozoic transpression and basin development, Kyrgyz Tien Shan. In Proceedings of the International Symposium, Moscow, Russia, 18–23 May 1996.
28. Cobbold, P.R.; Davy, P.; Gapais, D.; Rossello, E.A.; Sadybakasov, E.; Thomas, J.C.; Tondji Biyo, J.J.; de Urreiztieta, M. Sedimentary basins and crustal thickening. *Sediment. Geol.* **1993**, *86*, 77–89.
29. Duethmann, D.; Zimmer, J.; Gafurov, A.; Güntner, A.; Kriegel, D.; Merz, B.; Vorogushyn, S. Evaluation of areal precipitation estimates based on downscaled reanalysis and station data by hydrological modelling. *Hydrol. Earth Syst. Sci.* **2013**, *17*, 2415–2434.
30. Feld, C.; Haberland, C.; Schurr, B.; Sippl, C.; Wetzel, H.-U.; Roessner, S.; Ickrath, M.; Abdybachaev, U.; Orunbaev, S. Seismotectonic study of the Fergana region (southern Kyrgyzstan): Distribution and kinematics of local seismicity. *Earth Planets Space* **2015**, *67*, doi:10.1186/s40623-015-0195-1.
31. Haberland, C.; Abdybachaev, U.; Schurr, B.; Wetzel, H.; Roessner, S.; Sarnagoev, A.; Orunbaev, S.; Janssen, C. Landslides in southern Kyrgyzstan: Understanding tectonic controls. *Eos Trans. AGU* **2011**, *92*, 169–176.
32. Dodonov, A.E. Loess of Central Asia. *GeoJournal* **1991**, *24*, 185–194.
33. Havenith, H.B.; Torgoev, I.; Meleshko, A.; Alioshin, Y.; Torgoev, A.; Danneels, G. Landslides in the Mailuu-Suu Valley, Kyrgyzstan—Hazards and impacts. *Landslides* **2006**, *3*, 137–147.
34. Hooper, A. A multi-temporal InSAR method incorporating both persistent scatterer and small baseline approaches. *Geophys. Res. Lett.* **2008**, *35*, doi:10.1029/2008GL034654.
35. Berardino, P.; Fornaro, G.; Lanari, R.; Sansosti, E. A new algorithm for surface deformation monitoring based on small baseline differential SAR interferograms. *IEEE Trans. Geosci. Remote Sens.* **2002**, *40*, 2375–2383.
36. Hooper, A.; Zebker, H.A. Phase unwrapping in three dimensions with application to InSAR time series. *J. Opt. Soc. Am. A* **2007**, *24*, 2737–2747.
37. Farr, T.G.; Kobrick, M. Shuttle radar topography mission produces a wealth of data. *EOS Trans.* **2000**, *81*, 583–585.
38. Goldstein, R.M.; Werner, C.L. Radar interferogram filtering for geophysical applications. *Geophys. Res. Lett.* **1998**, *25*, 4035–4038.
39. Sousa, J.J.; Guimarães, P.; Sousa, A.; Ruiz, A.M.; Patrício, G.; Magalhães, L.; Pereira, F. Vistamps—A collaborative project for StaMPS/MTI results interpretation. *Procedia Technol.* **2014**, *16*, 842–848.

40. Bardi, F.; Frodella, W.; Ciampalini, A.; Bianchini, S.; del Ventisette, C.; Gigli, G.; Fanti, R.; Moretti, S.; Basile, G.; Casagli, N. Integration between ground based and satellite SAR data in landslide mapping: The San Fratello case study. *Geomorphology* **2014**, *223*, 45–60.
41. Cascini, L.; Fornaro, G.; Peduto, D. Advanced low- and full-resolution DInSAR map generation for slow-moving landslide analysis at different scales. *Eng. Geol.* **2010**, *112*, 29–42.
42. Colesanti, C.; Wasowski, J. Investigating landslides with space-borne Synthetic Aperture Radar (SAR) interferometry. *Eng. Geol.* **2006**, *88*, 173–199.
43. Chediya, O. *Morfostruktury I Noveishii Tektogenez Tyan'-Shanya (Morfostructures and Neotectonics of the Tien Shan)*; Ilim: Frunze/Bishkek, Kyrgyzstan, 1986.
44. Zhao, C.Y.; Lu, Z.; Zhang, Q.; de la Fuente, J. Large-area landslide detection and monitoring with ALOS/PALSAR imagery data over northern California and southern Oregon, USA. *Remote Sens. Environ.* **2012**, *124*, 348–359.
45. Hilley, G.E.; Bürgmann, R.; Ferretti, A.; Novali, F.; Rocca, F. Dynamics of slow-moving landslides from permanent scatterer analysis. *Science* **2004**, *304*, 1952–1955.
46. Agliardi, F.; Crosta, G.; Zanchi, A. Structural constraints on deep-seated slope deformation kinematics. *Eng. Geol.* **2001**, *59*, 83–102.
47. Kalmetieva, Z.; Mikolaichuk, A.; Moldobekov, B.; Meleshko, A.; Jantaev, M.; Zubovich, A.; Havenith, H. *Atlas of Earthquakes in Kyrgyzstan*; CAIAG: Bishkek, Kyrgyzstan, 2009.